

Engineering of *Saccharomyces pastorianus* Old Yellow Enzyme 1 for the Synthesis of Pharmacologically Active (*S*)-Profen Derivatives

Guigao Liu,^{1,‡} Shang Li,^{1,‡} Qinghua Shi,² Hengyu Li,² Jiyang Guo,² Jingping Ouyang,³ Xian Jia,³
Lihan Zhang,^{*,4} Song You,^{*,2} and Bin Qin^{*,1}

¹Wuya College of Innovation, Shenyang Pharmaceutical University, 103 Wenhua Road, Shenhe,
Shenyang 110016, People's Republic of China

²School of Life Sciences and Biopharmaceutical Sciences, Shenyang Pharmaceutical University,
103 Wenhua Road, Shenhe, Shenyang 110016, People's Republic of China

³School of Pharmaceutical Engineering, Shenyang Pharmaceutical University, 103 Wenhua
Road, Shenhe, Shenyang 110016, People's Republic of China

⁴School of Science, Westlake University, 18 Shilongshan Road, Xihu, Hangzhou 310024,
People's Republic of China

‡ G.L. and S.L. contributed equally.

*Corresponding author: to-qinbin@163.com (B.Q.); yousong206@aliyun.com (S.Y.);
zhanglihan@westlake.edu.cn (L.Z.).

Abstract

2-Arylpropionic acid derivatives, such as ibuprofen, constitute an important group of non-steroidal anti-inflammatory drugs (NSAIDs). Biocatalytic asymmetric reduction of 2-arylacrylic acid derivatives by ene reductases (EREDs) is a valuable approach for synthesis of these derivatives. However, previous bioreduction of 2-arylacrylic acid derivatives by either ERED wild-types or variants resulted solely in nonpharmacological (*R*)-enantiomers as the products. Here, we present the engineering of *Saccharomyces pastorianus* old yellow enzyme 1 (OYE1) into (*S*)-stereoselective enzymes, which afford pharmacologically active (*S*)-profen derivatives. By structural comparison of substrate recognition in related EREDs and analysis of non-covalent contacts in the pro-*S* model of OYE1, the key residues of OYE1 that switch its stereoselectivity to an (*S*)-stereopreference were identified. Systematic site-directed mutagenesis screening at these positions successfully provided the (*S*)-stereoselective OYE1 variants, which catalyzed stereoselective bioreduction of various profen precursors to afford pharmacologically active (*S*)-derivatives including (*S*)-ibuprofen and (*S*)-naproxen methyl esters with up to >99% *ee* values. Moreover, the key residues and mutation strategy obtained from OYE1 could be further transferred to OYE 2.6 (from *Pichia stipitis*) and KnOYE1 (from *Kazachstania naganishii*) to create the (*S*)-stereoselective EREDs. Our results may provide a generalizable strategy for stereocontrol of OYEs and set the basis for biocatalytic production of (*S*)-profens.

Keywords: ene reductases, profen, OYE1, biocatalysis, protein engineering

Introduction

Ene reductases (EREDs), which catalyze the reduction of activated C=C bonds and thus generate two chiral centers, are powerful and valuable biocatalysts in asymmetric synthesis.¹⁻⁵ Among the families of EREDs, the prototypical flavin mononucleotide (FMN)-containing old yellow enzymes (OYEs) catalyze bioreduction of a broad variety of substrates, including α , β -unsaturated aldehydes, ketones, esters, nitriles, and nitro compounds.^{1,4} The increasing studies on discovery and engineering of EREDs, and combining EREDs with chemocatalysis raise the potential for application of EREDs in pharmaceutical synthesis and organic synthesis.^{1-2,5-10}

The “profen” drugs, such as ibuprofen, flurbiprofen, ketoprofen, and naproxen, which have the 2-arylpropionic acid skeletons, belong to an important and frequently used group of non-steroidal anti-inflammatory drugs (NSAIDs). Although ibuprofen and ketoprofen are often used as racemic mixtures, the (*S*)-enantiomers of “profens” are the main bioactive enantiomers for cyclooxygenase (COX) inhibition, whereas the (*R*)-enantiomers are generally not considered as COX inhibitors. To prepare the optically pure (*S*)-profens, several biocatalytic methods have been tried in the past several decades.¹¹⁻²¹ The lipase-catalyzed kinetic resolution of racemic profen derivatives using wild-type (WT) or engineered enzymes is well studied in both industrial and lab scale, though the yield is theoretically limited to 50% at maximum.¹¹⁻¹⁴ An alternative approach is the use of alcohol dehydrogenases for dynamic kinetic resolution of tautomeric aldehyde derivatives, though this is only applicable to the production of chiral “profenols”.¹⁵ The dehydrogenase-mediate asymmetric disproportionation of aldehydes was further developed to produce (*S*)-profens, but the reaction efficiency is compromised by modest conversion rate and products being nearly 1:1 mixture of the profens and the profenols.¹⁶

The asymmetric C=C bond reduction of profen precursors by EREDs is an alternative and attractive biocatalytic route to prepare optically pure profens (**Figure 1**).^{1,17-21} Recent studies showed that some OYEs, such as YqjM (from *Bacillus subtilis*) and KYE2 (from *Kluyveromyces marxianus*), displayed the ability to stereoselectively reduce 2-arylacrylic acid methyl esters to afford (*R*)-2-arylpropionic acid methyl esters (**Figure 1a** and **Figure S1**).¹⁷⁻¹⁹ The Gröger group and Scrutton group also reported that several OYEs (GOx-ER from *Gluconobacter oxydans* and XenA from *Pseudomonas putida*) can catalyze the direct reduction of 2-arylacrylic acids, whose carboxyl moiety was previously thought to be too weak as an electron-withdrawing group for OYEs (**Figure 1a**).²⁰⁻²¹ Nevertheless, the bioreduction of profen precursors by the aforementioned wild-type OYEs gave the nonpharmacological (*R*)-enantiomers as the products (**Figure 1a** and **Figure S1**).¹⁷⁻²¹ Although some OYEs have been engineered into the (*S*)-selective enzymes in the reduction of carvones and other substrates (**Figure S2**),^{18,22-28} the challenge has remained for direct reductive production of (*S*)-profens.¹⁸ Herein, we report the engineering of ene reductase OYE1 (from *Saccharomyces pastorianus*) into (*S*)-selective enzymes, which can catalyze the stereoselective C=C bond reduction of various profen precursors to afford pharmacologically active (*S*)-profen derivatives, such as (*S*)-ibuprofen and (*S*)-naproxen methyl esters with up to >99% enantiomeric excess (*ee*) values (**Figure 1b**).

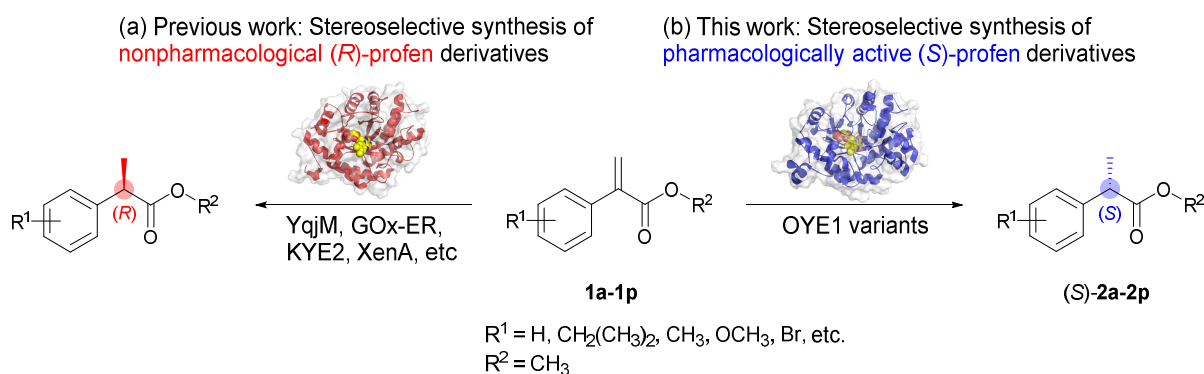


Figure 1. Asymmetric C=C bond bioreduction of 2-arylacrylic acid derivatives (profen precursors) by ene reductases (EREDs).

Results & discussion

In contrast to other reductive enzymes (e.g. ketoreductases), the studies on switching the stereopreference of EREDs are limited.^{1,26} We thus started from structural analyses of EREDs to better understand their stereochemical outcome and to design the binding mode for the unnatural pro-*S* orientation of 2-arylacrylic acid derivatives. A series of pioneering works by Stewart and Scrutton established the binding mode of OYE enzymes and proposed a “normal” binding mode and a “flipped” binding mode to explain the stereoselectivity (**Figure 2** and **Figure S2**).^{21,27-28} As shown in **Figure 2a**, the co-crystal structure of OYE1 W116L variant and the (4*R*)-carvone substrate (PDB:4GWE) shows a “normal” binding mode, where the larger moiety of (4*R*)-carvone that contains isopropenyl group is located in the left side of the binding pocket (pocket L) of OYE1 W116L variant to afford (1*R*,4*R*)-dihydrocarvone.²⁷ Similarly, the co-crystal structure of XenA with 2-phenylacrylic acid (PDB:5N6Q) shows that the larger phenyl group of 2-phenylacrylic acid is also positioned in the pocket L in a “normal” binding mode, which yields (*R*)-2-phenylpropionic acid as the product (**Figure 2c**).²¹ In contrast, in the OYE1 W116A variant, the (4*R*)-carvone substrate binds in a “flipped” mode, with the larger isopropenyl group located in the right side of the pocket (pocket R), which is created by the W116A substitution (**Figure 2b**).²⁷ This flipped orientation of (4*R*)-carvone would lead to the production of (1*S*,4*R*)-dihydrocarvone with the opposite stereochemistry at C1 position.²⁷ These analyses suggest that creating a “flipped” substrate binding mode²⁷⁻²⁸ by modifying the pockets L and R might be critical for the (*S*)-stereoselective reduction in EREDs.

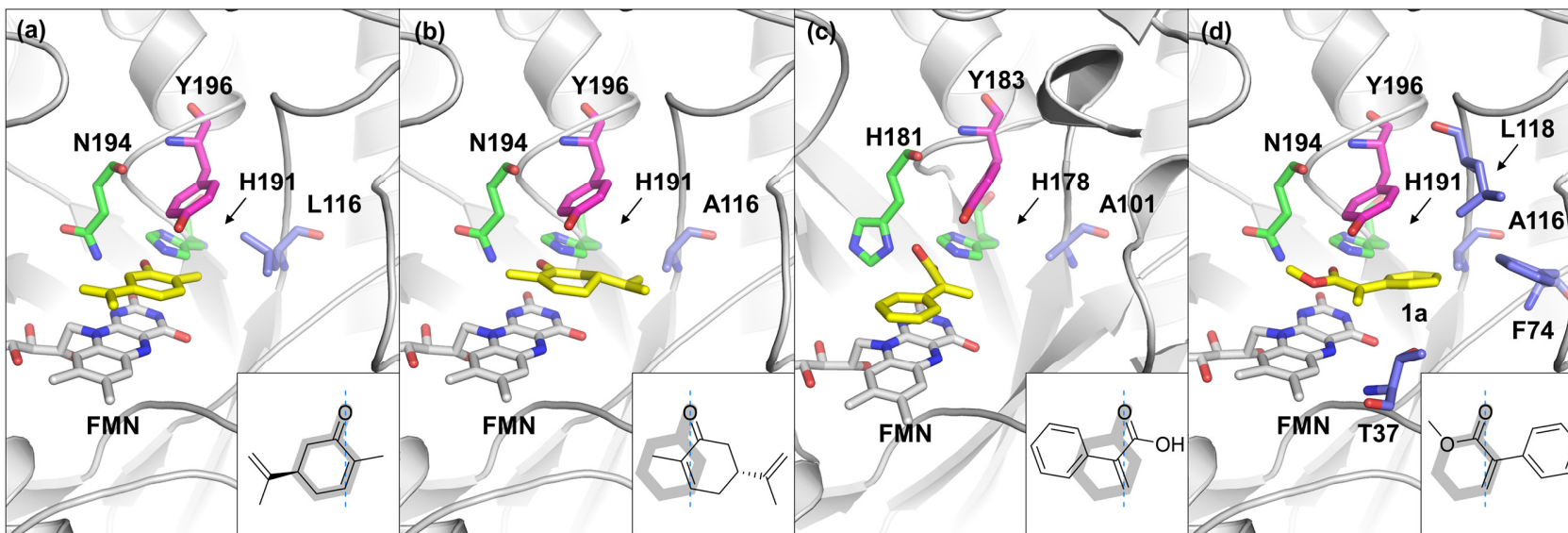


Figure 2. Structural comparison of reported (*R/S*)-stereoselective EREDs and the pro-*S* model of OYE1 with methyl 2-phenylacrylate (**1a**). FMN, the substrate, His/Asn (or His/His) catalytic diad, active site Tyr, and key residues forming the binding pocket R, are shown in white, yellow, green, magenta, and blue, respectively. The bottom right corner of each panel shows a simplified model of substrate recognition, with an asymmetry axis (blue dashed line) crossing the carbonyl oxygen (forming hydrogen bonds with enzymes) and β -carbon (accepting hydride from FMN). The gray highlight shows the comparison with “normal” binding of 2-cyclohexenone backbone²⁷⁻²⁸ (**Figure S2**). **(a)** OYE1 W116L with (4*R*)-carvone in a “normal” pro-*R* binding mode (PDB: 4GWE).²⁷ **(b)** OYE1 W116A with (4*R*)-carvone in a “flipped” pro-*S* binding mode (PDB: 4K7V).²⁷ **(c)** XenA with 2-phenylacrylic acid in a “normal” pro-*R* binding mode (PDB: 5N6Q).²¹ **(d)** OYE W116A with methyl 2-phenylacrylate (**1a**) in a “flipped” pro-*S* binding mode. This model was manually modified based on 4K7V with bound (4*R*)-carvone ligand,²⁷ then optimized by molecular dynamic simulation and the snapshot from MD trajectory was used for analysis.

To model the pro-*S* orientation of profen precursors, we manually modified the structure of (4*R*)-carvone in OYE1 W116A variant (PDB: 4K7V)²⁷ to methyl 2-phenylacrylate (**1a**, **Figure 2d** and **Table 1**) and optimized this model by molecular dynamic (MD) simulation. As show in **Figure 2d**, in a productive orientation from MD trajectory, the phenyl group of **1a** was positioned in the pocket R in a “flipped” manner, in contrast to the “normal” binding as observed in XenA (**Figure 2c**). Additionally, the carbonyl oxygen of **1a** is 2.3 Å and 2.4 Å from the side chains of H191 and N194, which is sufficient for formation of hydrogen bonds.²⁸⁻²⁹ Moreover, the *C* β and *C* α of **1a** is 3.5 Å and 3.0 Å from the N5 atom of FMN and the side chain of Y196, while the angle formed by FMN N10-N5-*C* β of **1a** is 107.0°, which is in a proper range for hydride attack.²⁸⁻²⁹ These evidences suggest that the OYE1 W116A variant may accept **1a** with a pro-*S* orientation in its binding pocket, and thus displays (*S*)-stereoselectivity in the asymmetric reduction of **1a**.

Next, to scrutinize the key amino acid interactions, we analyzed non-covalent contacts between the constructed pro-*S* model of substrate **1a** and residues of OYE1 W116A by the Protein Contacts Atlas online tool³⁰ (**Figure 3**). The result illustrated close contact between **1a** and the residues T37, M39, G72, F74, Y82, A85, A116, L118, Y375 (creating pocket R), and F250, P295, F296 (creating pocket L). In addition, residues T37, A116, F74, Y82, and L118 of pocket R displayed larger atomic contacts with **1a** (**Figure 3b**). On the basis of these observations, we hypothesized that protein engineering at these positions could reshape the binding pocket R (**Figure 3d**), which might switch the selectivity of OYE1 to the (*S*)-stereopreference and make it accept more bulky substrates.

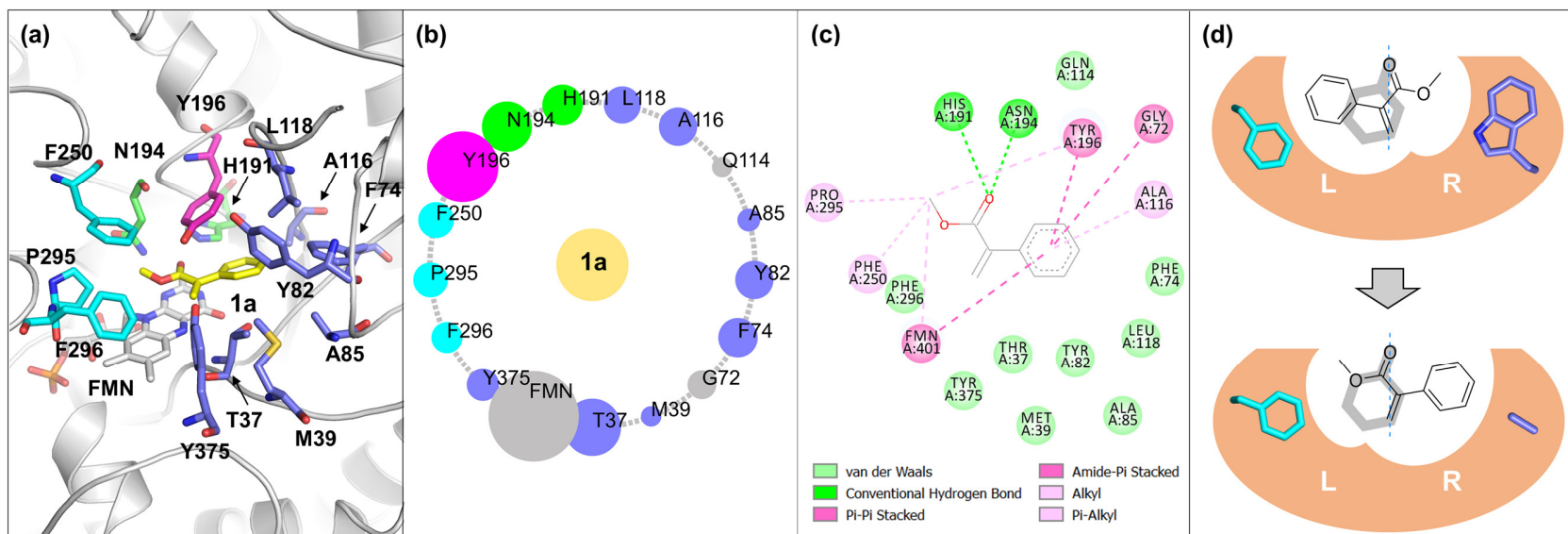
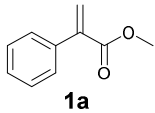
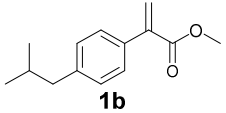
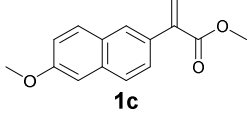
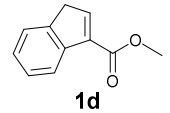


Figure 3. Analyses of the key residues and non-covalent contacts in the refined pro-*S* model of OYE1 W116A with methyl 2-phenylacrylate (**1a**). This model was constructed based on the modification of OYE1 W116A with bound (4*R*)-carvone (PDB: 4K7V).²⁷ **(a)** The pro-*S* model of OYE W116A with **1a**. The residues that create the left and the right binding pockets are shown in cyan and blue, respectively. **(b)** Non-covalent contacts of OYE1 W116A with **1a** that analyzed and visualized by the Protein Contacts Atlas online tool. Directly contacting residues are shown in the circle, while **1a** is shown as central node in the asteroid plot. The residues are colored according to different functions (green and magenta for catalytic residues, cyan for pocket L forming residues, and blue for pocket R forming residues), and the size of each circle is scaled to denote the strength of atomic contacts.³⁰ **(c)** Interaction between OYE1 W116A and **1a** analyzed by the Discovery Studio Visualizer. The residues are colored according to different types of interactions. **(d)** Simple models of pro-*R* OYE1 (top) and pro-*S* OYE1 (bottom).

Table 1. Asymmetric Reduction of 2-Arylacrylic Acid Derivatives 1a–1d by YqjM, OYE1, and OYE1 Variants.

ERED	 1a	 1b	 1c	 1d
YqjM WT	>99 ^a , >99 ^b (<i>R</i>) ^c	77.2, 98.3 (<i>R</i>)	97.8, >99 (<i>R</i>)	96.4, >99 (<i>R</i>)
OYE1 WT	96.9, >99 (<i>R</i>)	88.0, 97.5 (<i>R</i>)	97.1, >99 (<i>R</i>)	50.0, >99 (<i>R</i>)
OYE1 W116G	98.2, 78.4 (<i>S</i>)	NA	NA	52.3, 49.5 (<i>S</i>)
OYE1 W116A	77.9, 81.4 (<i>S</i>)	NA	NA	98.6, 49.6 (<i>S</i>)
OYE1 W116V	NA ^d	NA	NA	NA
OYE1 W116S	73.4, 56.7 (<i>R</i>)	NA	NA	38.9, 82.4 (<i>R</i>)
OYE1 W116A/T37G	30.9, 91.6 (<i>S</i>)	NA	NA	98.5, >99 (<i>S</i>)
OYE1 W116A/T37A	>99, 98.1 (<i>S</i>)	NA	NA	99.4, >99 (<i>S</i>)
OYE1 W116A/T37V	66.9, 95.7 (<i>S</i>)	NA	NA	NA
OYE1 W116A/T37S	28.0, 92.3 (<i>S</i>)	NA	NA	96.9, 91.7 (<i>S</i>)
OYE1 W116A/T37A/F74G	32.1, 80.4 (<i>S</i>)	3.6, 96.6 (<i>S</i>)	5.6, 96.8 (<i>S</i>) ^e	29.2, 89.8 (<i>S</i>)
OYE1 W116A/T37A/F74A	>99, 95.4 (<i>S</i>)	4.6, 96.6 (<i>S</i>)	4.1, 89.7 (<i>S</i>) ^e	99.2, 91.9 (<i>S</i>)
OYE1 W116A/T37A/F74V	26.3, 94.1 (<i>S</i>)	12.7, 96.7 (<i>S</i>)	NA	57.0, 97.7 (<i>S</i>)
OYE1 W116A/T37A/F74S	35.3, 96.3 (<i>S</i>)	13.2, 97.7 (<i>S</i>)	NA	86.1, 89.8 (<i>S</i>)
OYE1 W116G/T37A/F74A	NA	68.5, 99.4 (<i>S</i>)	4.2, 89.1 (<i>S</i>) ^e	33.9, 53.6 (<i>S</i>)
OYE1 W116A/T37A/F74A/L118A	NA	92.9, 97.4 (<i>S</i>)	60.0, 93.1 (<i>S</i>) ^e	NA
OYE1 W116G/T37A/F74A/L118A	NA	19.0, 97.3 (<i>S</i>)	95.9, 99.7 (<i>S</i>)^e	NA

^aThe conversions in percent were determined by chiral HPLC analysis. ^bThe enantiomeric excess (*ee*) values of resultant products in percent were measured by chiral HPLC analysis. ^cThe absolute configurations of the resultant products were identified by comparing the retention times of chiral HPLC with authentic samples, literature data, or the different stereopreferences of YqjM and OYE1 variants (Table S2 in the Supplementary Information). ^dNA, no measurable activity. ^eReaction was performed using the purified enzyme (See Supplementary Information for details). Reaction condition: The reactions were carried out at analytical scale using the cell lysate of *E. coli* expressing EREDs (0.2 g wet cells) and GDH (0.1 g wet cells) with substrate (3 mM, in 50 μ L EtOH or DMSO), glucose (44 mM), NADP⁺ (0.4 mM), and PBS buffer (100 mM, pH 7.0, 950 μ L) at 30 °C, stirring at 200 rpm for 24 h. For reactions using purified enzymes, the reactions were carried out using purified EREDs (10 μ M) with **1c** (3 mM, in 50 μ L DMSO) and NADPH (6 mM) at 30 °C and 200 rpm for 24 h.

To test the above hypothesis of “flipped” binding mode controlled by the left and the right pocket size, we first focused on the W116 position of OYE1. While our pro-*S* model of OYE1 was prepared based on the W116A variant, we systematically mutated the residue 116 with amino acids Gly, Ala, Val, and Ser to investigate the size effect of the side chain’s size (namely shrinkage scanning hereafter). As shown in **Table 1**, in accordance with the stereoselectivity of characterized wild-type EREDs, YqjM WT and OYE1 WT displayed high (*R*)-stereoselectivity toward **1a**, yielding methyl (*R*)-2-phenylpropanoate (**2a**) with >99% *ee* values. In contrast, the reduction of **1a** by OYE1 W116G and W116A variants gave the product **2a** with an *S* configuration. Although the (*S*)-stereoselectivity of OYE1 variants toward **1a** was not high enough (78.4% *ee* for W116G variant and 81.4% *ee* for W116A variant), this result revealed that the bulky phenyl group of **1a** was located with a “flipped”, pro-*S* conformation in the enlarged pocket R created by the W116G/A substitutions. In case of the W116V and W116S variants, the slightly larger side chain of Val and polar Ser might disfavor the positioning of the substrate’s phenyl group in pocket R, leading to the loss of activity and the (*R*)-stereoselectivity, respectively.

Having established a mutant with modest (*S*)-stereoselectivity against the profen substrate analog, we aimed to improve the stereoselectivity by structure-guided rational design. We noticed that the residue T37 of the pocket R (**Figure 3b**) had the largest non-covalent contacts (except catalytic Y196) with **1a**. The polar side chain of T37 could disfavor the orientation of the phenyl group of **1a** in this region, which might have decreased the (*S*)-stereoselectivity. Although the conserved T37 (**Figure S3**) was previously known to be important for catalytic activity,³¹ our recent study on engineering the T37 of OYE1 toward (4*R*)-carvone³² and other studies of engineering the corresponding C26 residue (of YqjM) in classical and thermophilic-like OYEs³³⁻³⁴ indicated the mutability at this position. Therefore, the shrinkage scanning with Gly, Ala, Val,

or Ser substitutions was also applied to the residue T37 of the OYE1 W116A variant. As shown in **Table 1**, enhanced (*S*)-stereoselectivity was found in asymmetric reduction of **1a** by all the constructed variants. Notably, the OYE1 W116A/T37A variant displayed the highest activity and selectivity toward **1a**, yielding methyl (*S*)-2-phenylpropanoate ((*S*)-**2a**) as the product with a 98.1% *ee* value.

Motivated by these results, we next tried the biocatalytic reduction of methyl 2-(4-isobutylphenyl)acrylate (**1b**) and methyl 2-(6-methoxynaphthalen-2-yl)acrylate (**1c**), which are the precursors of ibuprofen and naproxen, respectively. Unfortunately, the OYE1 W116A/T37A variant and the other T37 variants did not show any activity toward **1b** and **1c** (**Table 1**). We then constructed the pro-*S* models of OYE1 W116A/T37A with **1b** and **1c** (**Figure S4**) to identify a potential clash in the pocket R with substrates. The model indicated that the bulky side chain of F74 can block the bulkier aryl moiety of **1b/1c**. Moreover, since the F74 position in homologues of OYE1 showed several variants at this position (**Figure S3**), we targeted F74 by the shrinkage scanning with the aim of creating a larger pocket R for the binding of these bulky substrates. The resulting four mutants, although with low activity, displayed high (*S*)-stereoselectivity in the asymmetric reduction of **1b**, and the F74G and F74A mutants even accepted **1c** with 90% stereoselectivity. The OYE1 W116A/T37A/F74A variant was next selected for further mutation rather than the F74G variant since the F74A substitution might stabilize the substrate binding by alkyl interaction. The L118 residue forming the pocket R was also mutated to smaller Ala with the intent to further enlarge the pocket R. As shown in **Table 1**, the conversion rate of the OYE1 W116A/T37A/F74A/L118A variant toward the ibuprofen analog **1b** was dramatically improved to 92.9% from 4.9%, while the (*S*)-stereoselectivity was maintained at high (97.4% *ee*). The conversion rate of the OYE1 W116A/T37A/F74A/L118A variant toward the naproxen analog **1c**

was further improved to 95.9% by an Ala to Gly mutation (W116G/T37A/F74A/L118A variant) with an excellent 99.7% *ee* value for the (*S*)-enantiomer. To the best of our knowledge, these results demonstrate the first OYE enzymes capable of producing (*S*)-profen derivatives.

In addition, we also investigated the asymmetric reduction of substrate **1d**, whose reduction product was previously used as the precursor for the synthesis of human peptidyl-prolyl-*cis/trans*-isomerase (Pin1) inhibitors.³⁵ The binding mode of **1d** in the pocket R of the OYE1 W116A variant was similar as that of **1a**, albeit its bicyclic structure, making it a promising substrate for asymmetric reduction (**Figure S5**). As shown in **Table 1**, the OYE1 WT displayed a high (*R*)-stereoselectivity toward **1d** with a >99% *ee* value, whereas the OYE1 W116A/T37A variant exhibited a high (*S*)-stereoselectivity ((*S*)-**2d** with a >99% *ee* value). Consistent with our modeling prediction, the stereochemical preference was identical between **1a** and **1d** across all OYE1 variants we tested. These results also indicated that the stereocomplementary reduction of **1d** was achieved through the OYE1 WT and the obtained OYE1 variants.

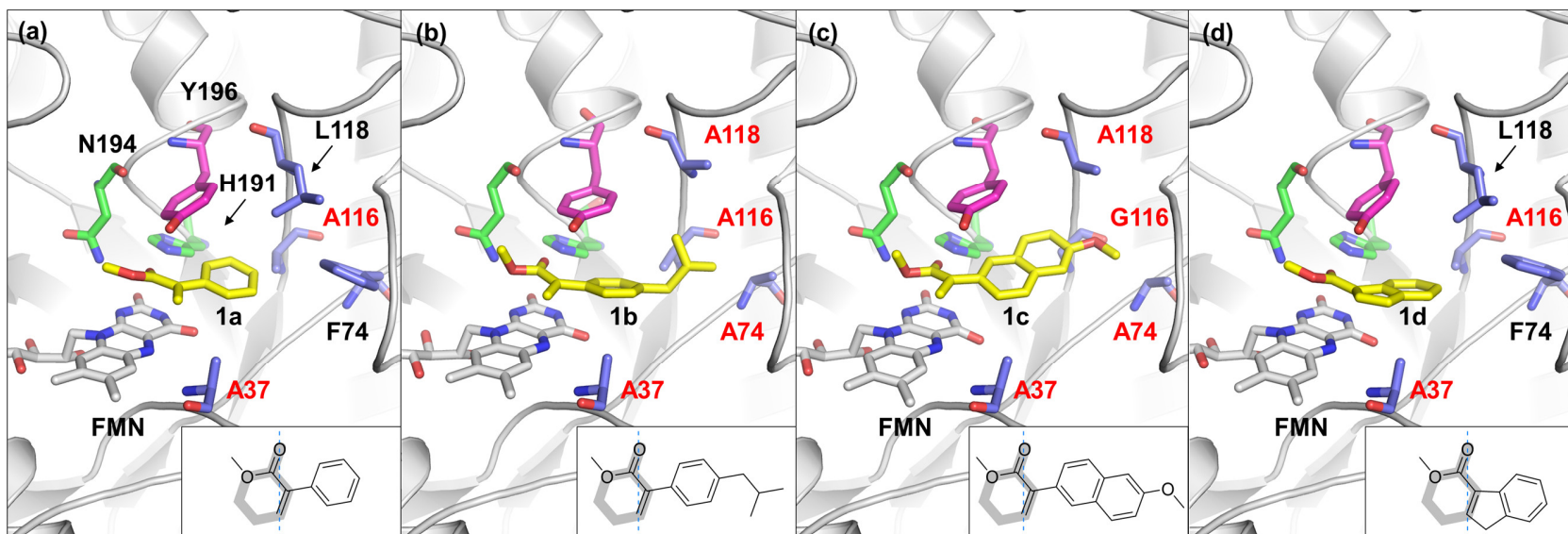


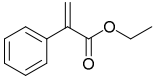
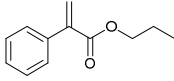
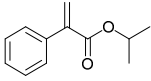
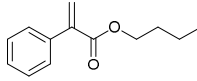
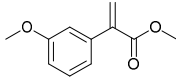
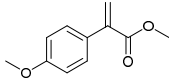
Figure 4. Results from the MD simulation of OYE1 variants with corresponding substrates. **(a)** Snapshot of the MD trajectory for OYE1 W116A/T37A variant with methyl 2-phenylacrylate (**1a**). Key residues in the binding pocket R are shown as blue sticks and labels for mutations are shown in red. **(b)** Snapshot of the MD trajectory for OYE1 W116A/T37A/F74A/L118A variant with methyl 2-(4-isobutylphenyl)acrylate (**1b**, ibuprofen precursor). **(c)** Snapshot of the MD trajectory for OYE1 W116G/T37A/F74A/L118A variant with methyl 2-(6-methoxynaphthalen-2-yl)acrylate (**1c**, naproxen precursor). **(d)** Snapshot of the MD trajectory for OYE1 W116A/T37A variant with methyl 1H-indene-3-carboxylate (**1d**, precursor of Pin1 inhibitors³⁵).

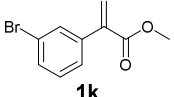
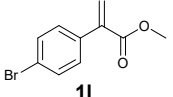
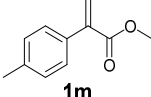
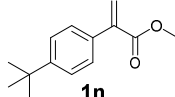
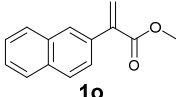
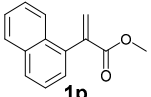
To scrutinize the molecular basis of the (*S*)-stereoselectivity of the OYE1 variants, four pro-*S* models of the OYE1 variants, W116A/T37A with **1a**, W116A/T37A/F74A/L118A with **1b**, W116G/T37A/F74A/L118A with **1c**, and W116A/T37A with **1d** were constructed and then optimized by molecular dynamics simulations. Analyses of the distance between the carbonyl oxygen of the substrate and the side chains of H191/N194, the distance between the $C\beta/C\alpha$ of the substrate and FMN-N5 or Y196, and the angle of FMN and substrate ($N10-N5-C\beta$) indicated that most models were stable and some orientations were productive (**Figure 4** and **Figure S6**). For example, the stability of OYE1 W116A variant with **1a** was improved by the W116A/T37A variant, which might explain the improved (*S*)-stereoselectivity. Although the stability of the W116A/T37A/F74A/L118A with **1b** was lower than that of the W116G/T37A/F74A/L118A with **1c**, enhanced stability was found in the W116G/T37A/F74A/L118A variant toward **1b**, which also displayed a high (*S*)-selectivity toward **1b**. Moreover, the calculated volume of substrate binding pockets (by CASTp 3.0)³⁶ revealed that the shrinkage mutations W116G/A, T37A, F74A, and L118A have contributed to the enlarged binding pocket volume (**Figure S7**). In addition, the analysis of non-covalent contacts indicated that the newly generated π -alkyl or alkyl-alkyl interactions between the introduced residue substitutions (W116A, T37A, F74A, or L118A) and substrates could stabilize the binding of substrates, which might contribute to the better “flipped” binding mode required for the (*S*)-stereoselectivity (**Figure 4** and **Figure S8**). We also compared the structure of the (*R*)-stereopreferred XenA²¹ and the model of OYE1 W116A/T37A to understand the unique (*S*)-selectivity of the obtained OYE1 variants. Although XenA does have an A101 residue that corresponds to the W116 in OYE1 and smaller residues at the sites corresponding to T37, F74, and L118 in the pocket R of OYE1 (**Figure S9**), the loops $\beta11/\alpha7$ and $\beta10/\alpha6$ of XenA are slightly away from its substrate binding pocket, resulting in an open pocket L

(**Figure S10**). In contrast, the equivalent loops $\beta 11/\alpha 10$ and $\beta 10/\alpha 9$ of OYE1 are closer around the substrate binding pocket, and the volume of pocket L is restricted by the residues F250, P295, and F296 in these loops (**Figure S10**). Thus, the restricted pocket L of OYE1 might promote the bulky phenyl group of the substrates to locate in the enlarged pocket R created by the W116A and T37A substitutions, leading to the (*S*)-stereoselectivity.

Next, we explored the substrate scope of the obtained (*S*)-stereoselective OYE1 variants. To evaluate the contribution of pocket L and pocket R in substrate recognition, we prepared a range of substitutions in the ester moiety and the aryl moiety of the substrates (**1e-1p**) and tested them against YqjM and OYE1 (**Table 2**). In agreement with our hypothesis and previously reported stereoselectivity, YqjM and OYE1 WT exhibited an (*R*)-stereoselectivity toward all accepted substrates, whereas the OYE1 variants exhibited an (*S*)-stereoselectivity to a variety of substrates that have modified aryl group (**1i-1o**) with high to excellent selectivity. Notably, the triple mutations W116G/T37A/F74A were essential to accommodate *p*-substituted substrates (**1j, 1l-1n**) in a “flipped” manner in pocket R. The substrates with longer ester side chain (**1f-1h**) were not accepted by YqjM and OYE1 WT presumably due to the limited size of their binding pocket, and we observed an (*R*)-stereoselectivity even with the engineered OYE1 W116A/T37A mutant for **1f** and **1h**. This was reasonable because the longer propyl and butyl ester may clash with the small pocket L, thus flipping back the substrate to the “normal” binding mode, with longer ester moiety positioned in the enlarged pocket R. None of the enzymes displayed activity toward **1g** and **1p**, indicating the substrate size limit for these OYE1 variants.

Table 2. Asymmetric Reduction of 2-Arylacrylic Acid Derivatives 1e–1p by YqjM, OYE1, and Selected OYE1 Variants.

ERED	 1e	 1f	 1g	 1h	 1i	 1j
YqjM WT	5.4 ^a , 98.2 ^b (<i>R</i>)	NA	NA	NA	>99, >99 (<i>R</i>)	>99, >99 (<i>R</i>)
OYE1 WT	NA	NA	NA	NA	>99, >99 (<i>R</i>)	>99, >99 (<i>R</i>)
OYE1 selected variant (Variant)	94.2, 89.2 (<i>S</i>) (W116A/T37A)	42.7, 78.9 (<i>R</i>) (W116A/T37A)	NA	91.6, 93.3 (<i>R</i>) (W116A/T37A)	>99, 97.7 (<i>S</i>) (W116A/T37A)	>99, 99.8 (<i>S</i>) (W116G/T37A/F 74A)

EREDs	 1k	 1l	 1m	 1n	 1o	 1p
YqjM WT	>99, >99 (<i>R</i>)	>99, >99 (<i>R</i>)	>99, >99 (<i>R</i>)	94.7, >99 (<i>R</i>)	96.7, >99 (<i>R</i>)	NA
OYE1 WT	>99, >99 (<i>R</i>)	>99, >99 (<i>R</i>)	>99, >99 (<i>R</i>)	57.2, >99 (<i>R</i>)	88.4, >99 (<i>R</i>)	NA
OYE1 selected variant (Variant)	>99, >99 (<i>S</i>) (W116A/T37A)	>99, >99 (<i>S</i>) (W116G/T37A/F 74A)	>99, >99 (<i>S</i>) (W116G/T37A/F 74A)	91.5, >99 (<i>S</i>) (W116G/T37A/F 74A)	81.8, 90.8 (<i>S</i>) (W116G/T37A/F 74A)	NA

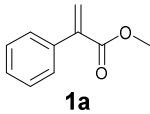
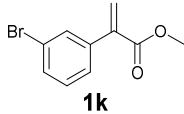
^aThe conversions in percent, determined by chiral HPLC analysis. ^bThe enantiomeric excess (*ee*) values of resultant products in percent, measured by chiral HPLC analysis. Reaction condition: The reactions were carried out at analytical scale using the cell lysate of *E. coli* expressing EREDs (0.2 g wet cells) and GDH (0.1 g wet cells) with substrate (3 mM, in 50 μ L EtOH or DMSO), glucose (44 mM), NADP⁺ (0.4 mM), and PBS buffer (100 mM, pH 7.0, 950 μ L) at 30 $^{\circ}$ C, stirring at 200 rpm for 24 h.

Table 3. Kinetic Parameters of OYE1 WT and Variants toward 2-Arylacrylic Acid Derivatives.

Substrate	ERED	K_m [mM]	k_{cat} [s ⁻¹]	k_{cat}/K_m [mM ⁻¹ s ⁻¹]
1a	WT	5.05 ± 0.56	0.10 ± 0.06	0.019
	W116A/T37A	11.09 ± 4.8	0.26 ± 0.08	0.024
1b	W116A/T37A/F74A/L118A	0.37 ± 0.06	0.016 ± 0.001	0.045
1c	W116G/T37A/F74A/L118A	2.49 ± 2.3	0.031 ± 0.026	0.013
1i	WT	2.42 ± 0.84	0.040 ± 0.007	0.016
	W116A/T37A	1.05 ± 0.53	0.042 ± 0.008	0.040
1j	WT	4.05 ± 0.48	0.035 ± 0.002	0.0088
	W116G/T37A/F74A	5.87 ± 0.89	0.047 ± 0.005	0.0081
1k	WT	2.81 ± 0.52	0.063 ± 0.008	0.022
	W116A/T37A	1.29 ± 0.56	0.16 ± 0.04	0.12
1l	WT	1.20 ± 0.19	0.094 ± 0.008	0.078
	W116G/T37A/F74A	0.62 ± 0.25	0.028 ± 0.005	0.045

The kinetic assays were carried out in 200 μ L PBS buffer (100 mM, pH 7.0) containing FMN (12.5 μ M), NADPH (1.5 mM), glucose oxidase (*ca.* 10 U), glucose (50 mM), at 30 °C using 5.6 μ M to 7.4 μ M of the OYEs at substrate concentrations ranging from 0.15 mM to 6.6 mM.

Table 4. Asymmetric Reduction of 2-Arylacrylic Acid Derivatives 1a and 1k by OYE1, OYE2.6, KnOYE1 and Their Variants.

ERED	 1a	 1k
OYE1 WT	96.9 ^a , >99 ^b (<i>R</i>)	>99, >99 (<i>R</i>)
OYE1 W116A	77.9, 81.4 (<i>S</i>)	85.3, 72.6 (<i>S</i>)
OYE1 W116A/T37A	>99, 98.1 (<i>S</i>)	>99, >99 (<i>S</i>)
OYE2.6 WT	NA	13.0, 94.7 (<i>R</i>)
OYE2.6 I113A	53.4, 49.1 (<i>S</i>)	94.3, 75.1 (<i>S</i>)
OYE2.6 I113A/T35A	NA	12.7, 75.8 (<i>S</i>)
OYE2.6 N293F/I113A	35.0, 45.4 (<i>S</i>)	83.9, 80.9 (<i>S</i>)
OYE2.6 N293F/I113A/T35A	NA	99.4, 99.4 (<i>S</i>)
KnOYE1 WT	NA	4.1, 94.4 (<i>R</i>)
KnOYE1 R119A	>99, 92.4 (<i>R</i>)	>99, 85.4 (<i>R</i>)
KnOYE1 R119A/T40A	NA	74.8, 0.9 (<i>R</i>)
KnOYE1 S299F/R119A	92.0, 74.0 (<i>R</i>)	90.2, 24.8 (<i>R</i>)
KnOYE1 S299F/R119A/T40A	24.0, 84.4 (<i>S</i>)	30.1, 67.7 (<i>S</i>)
KnOYE1 S299F/R119A/T40A/W42A	>99, 70.0 (<i>S</i>)	94.6, 79.7 (<i>S</i>)

^aThe conversions in percent, determined by chiral HPLC analysis. ^bThe enantiomeric excess (*ee*) values of resultant products in percent, measured by chiral HPLC analysis. Reaction condition: The reaction was carried out at analytical scale using the cell lysate of *E. coli* expressing EREDs (0.2 g wet cells) and GDH (0.1 g wet cells) with substrate (3 mM, in 50 μ L EtOH or DMSO), glucose (44 mM), NADP⁺ (0.4 mM), and PBS buffer (100 mM, pH 7.0, 950 μ L) at 30 °C, stirring at 200 rpm for 24 h.

The kinetic studies of the OYE1 WT and variants with selected substrates were also carried out to investigate the catalytic efficiency. As shown in **Table 3**, the OYE1 W116A/T37A variant displayed higher catalytic efficiency ($k_{\text{cat}}/K_{\text{m}}$) than the WT enzyme against **1a**, **1i**, and **1k**. Notably, the highest catalytic efficiency was found in the bioreduction of **1k** by the W116A/T37A variant. Overall, the OYE1 variants producing the (*S*)-profen derivatives exhibited comparable catalytic efficiency to the (*R*)-stereoselective OYE1 WT, demonstrating the robustness of the engineered variants. The aryl moiety of the substrates could also influence the activity, as both WT and the variants displayed higher catalytic efficiency against the *p*-/*m*-Br substituted substrates (**1k** and **1l**) than that against the *p*-/*m*-OMe substituted substrates (**1i** and **1j**). The OYE1 variants have modest changes in both K_{m} and k_{cat} values when compared with the WT or against different substrates, suggesting their complicated effects in substrate binding and reaction turnover.

To determine the yield of the OYE-catalyzed (*S*)-profen production, we used substrates **1b**, **1d**, **1i**, **1j**, and **1l**, for biocatalytic C=C bond reduction by the appropriate OYE1 variants. With 0.08 mmol of the substrates, we furnished (*S*)-**2b**, (*S*)-**2d**, (*S*)-**2i**, (*S*)-**2j**, and (*S*)-**2l** in 16-31% isolated yields. The low yields are presumably due to the loss of products during the extraction and purification process. In the enlarged reactions on 0.19 mmol for **1a** and 1.0 mmol for **1k**, the OYE1 W116A/T37A variant delivered (*S*)-**2a** and (*S*)-**2k** in improved 66% (98% *ee*) and 68% (99% *ee*) yields, respectively, which raises the potential applications of these (*S*)-stereopreferred OYEs.

Finally, with the OYE1 variants that could prepare the pharmacologically active (*S*)-profen derivatives in hand, we turned to find and engineer more EREDs with an (*S*)-stereopreference toward profen precursors. BLAST search and multiple-sequence alignment of OYE1 homologues revealed that the W116 and T37 were highly conserved among these enzymes (**Figure S3**), which might explain why most EREDs show an (*R*)-stereopreference. Notably, OYE2.6 (from *Pichia*

stipitis) is known to display an (*S*)-stereopreference toward a series of substrates and has the Ile113 (corresponding to W116 of OYE1, **Figure S11** and **Figure S12**).³⁷⁻³⁸ Additionally, we identified KnOYE1 from *Kazachstania naganishii* by genome mining (NCBI accession: XP_022464309), which has a 63% sequence identity with OYE1 and contains an Arg residue at the 119 position (corresponding to the W116 position of OYE1, **Figure S11** and **Figure S12**). We tested the two enzymes using compounds **1a** and **1k** to investigate whether the mutation corresponding to the W116 of OYE1 can yield the (*S*)-stereopreference. Although OYE2.6 WT and KnOYE1 WT did not show activity toward **1a**, introduction of the I113A mutation in analogy to the OYE1 W116A, with the aim of expanding the pocket R in OYE2.6 resulted in the (*S*)-stereoselective reduction of **1a** (**Table 4**). However, the equivalent mutations R119A and R119A/T40A in KnOYE1 did not show the (*S*)-stereopreference toward **1a**, suggesting that expansion of the pocket R is not enough for accommodating the substrate. To facilitate substrate binding in the pocket R of KnOYE1, we designed the S299F mutation to limit the size of pocket L, and the W42A mutation to enlarge the pocket R (**Figure S12**). The assay results revealed that a combination of mutations in pocket L (S299F) and pocket R (T40A/W42A) effectively converted the stereoselectivity from (*R*)- to (*S*)-form toward **1a**. For substrate **1k**, the enhanced (*S*)-stereoselectivity was found in related OYE2.6 variants with further mutation of N293F (corresponding to the F296 of OYE1 and S299 of KnOYE1). Similarly, the S299F and W42A substitution also contributed to the (*S*)-stereopreference of KnOYE1 variants toward **1k**. These results suggest that the rational binding site design of the pockets L and R can be a general strategy to modify the stereoselectivity of OYE family enzymes.

Conclusions

Biocatalytic reduction of the C=C bonds of 2-arylacrylic acid derivatives by EREDs is an attractive route to synthesize optically pure profens. However, most EREDs catalyzed asymmetric reactions display the same stereoselectivity, yielding the nonpharmacological (*R*)-profen derivatives as the products, which limits further application of EREDs. In this research, we engineered OYE1 into (*S*)-stereoselective enzymes that could synthesize the pharmacologically active (*S*)-profen derivatives by asymmetric reduction of the prochiral precursors. Through careful comparison of the substrate recognition in structures of EREDs and analysis of the non-covalent contacts in the pro-*S* model of OYE1 with substrate, the key residues in the binding pocket R that control stereoselectivity were identified in OYE1. Expanding the substrate binding pocket R of OYE1 by mutagenesis with smaller substitutions at these residues switched its (*R*)-stereoselectivity to (*S*)-stereoselectivity, resulting in the production of (*S*)-ibuprofen, (*S*)-naproxen, and other (*S*)-2-arylpropionic acid derivatives with up to >99% *ee* values. Furthermore, mutagenesis of OYE2.6 and KnOYE1 at the positions corresponding to OYE1 successfully switched their stereopreferences to the (*S*)-form toward 2-arylacrylic acid derivatives. Although our study remains in laboratory-scale biocatalysis, the OYEs mediated reductions on preparative scale have been reported recently, for example including the reduction of methyl-3-oxocyclohex-1-enecarboxylate in an astonishing 100-gram scale.^{3,5,39} The generalizable binding site design strategy in this research and the obtained (*S*)-stereoprefered EREDs will set the basis for the application of related biocatalysts.

Conflicts of interest

There are no conflicts to declare

Acknowledgment

This work was financially supported by the National Natural Science Foundation of China (31971207, 81602993), LiaoNing Revitalization Talents Program (XLYC1907153), and Young Elite Scientists Sponsorship Program by CAST (2016QNRC001).

References

- (1) H. S. Toogood and N. S. Scrutton, *ACS Catal.*, 2018, **8**, 3532-3549.
- (2) P. N. Devine, R. M. Howard, R. Kumar, M. P. Thompson, M. D. Truppo and N. J. Turner, *Nat. Rev. Chem.*, 2018, **2**, 409-421.
- (3) C. K. Winkler, K. Faber and M. Hall, *Curr. Opin. Chem. Biol.*, 2018, **43**, 97-105.
- (4) M. Hall and A. S. Bommarius, *Chem. Rev.*, 2011, **111**, 4088-4110.
- (5) F. Hollmann, D. J. Opperman and C. E. Paul, *Angew. Chem., Int. Ed.*, 2020, DOI: 10.1002/anie.202001876.
- (6) Z. C. Litman, Y. Wang, H. Zhao and J. F. Hartwig, *Nature*, 2018, **560**, 355-359.
- (7) X. Huang, B. Wang, Y. Wang, G. Jiang, J. Feng and H. Zhao, *Nature*, 2020, **584**, 69-74.
- (8) K. F. Biegasiewicz, S. J. Cooper, X. Gao, D. G. Oblinsky, J. H. Kim, S. E. Garfinkle, L. A. Joyce, B. A. Sandoval, G. D. Scholes and T. K. Hyster, *Science*, 2019, **364**, 1166-1169.
- (9) B. A. Sandoval, S. I. Kurtoic, M. M. Chung, K. F. Biegasiewicz and T. K. Hyster, *Angew. Chem., Int. Ed.*, 2019, **58**, 8714-8718.

- (10) T. W. Thorpe, S. P. France, S. Hussain, J. R. Marshall, W. Zawodny, J. Mangas-Sanchez, S. L. Montgomery, R. M. Howard, D. S. B. Daniels, R. Kumar, F. Parmeggiani and N. J. Turner, *J. Am. Chem. Soc.*, 2019, **141**, 19208-19213.
- (11) R. Kourist, P. Domínguez de María and K. Miyamoto, *Green Chem.*, 2011, **13**, 2607-2618.
- (12) A. G. Sandström, Y. Wikmark, K. Engström, J. Nyhlén and J.-E. Bäckvall, *Proc. Natl. Acad. Sci. U. S. A.*, 2012, **109**, 78-83.
- (13) Q. Wu, P. Soni and M. T. Reetz, *J. Am. Chem. Soc.*, 2013, **135**, 1872-1881.
- (14) B. Qin, P. Liang, X. Jia, X. Zhang, M. Mu, X.-Y. Wang, G.-Z. Ma, D.-N. Jin and S. You, *Catal. Commun.*, 2013, **38**, 1-5.
- (15) J. A. Friest, Y. Maezato, S. Broussy, P. Blum and D. B. Berkowitz, *J. Am. Chem. Soc.*, 2010, **132**, 5930-5931.
- (16) E. Tassano, K. Faber and M. Hall, *Adv. Synth. Catal.*, 2018, **360**, 2742-2751.
- (17) J. Pietruszka and M. Schölzel, *Adv. Synth. Catal.*, 2012, **354**, 751-756.
- (18) E. Rühllein, T. Classen, L. Dobnikar, M. Schölzel and J. Pietruszka, *Adv. Synth. Catal.*, 2015, **357**, 1775-1786.
- (19) Z. Li, Z. Wang, G. Meng, H. Lu, Z. Huang and F. Chen, *Asian J. Org. Chem.*, 2018, **7**, 763-769.
- (20) T. Reiß, W. Hummel, S. P. Hanlon, H. Iding and H. Gröger, *ChemCatChem*, 2015, **7**, 1302-1311.
- (21) J. Waller, H. S. Toogood, V. Karuppiyah, N. J. W. Rattray, D. J. Mansell, D. Leys, J. M. Gardiner, A. Fryszkowska, S. T. Ahmed, R. Bandichhor, G. P. Reddy and N. S. Scrutton, *Org. Biomol. Chem.*, 2017, **15**, 4440-4448.

- (22) E. Brenna, M. Crotti, F. G. Gatti, D. Monti, F. Parmeggiani, R. W. Powell Iii, S. Santangelo and J. D. Stewart, *Adv. Synth. Catal.*, 2015, **357**, 1849-1860.
- (23) A. B. Daugherty, S. Govindarajan and S. Lutz, *J. Am. Chem. Soc.*, 2013, **135**, 14425-14432.
- (24) A. B. Daugherty, J. R. Horton, X. Cheng and S. Lutz, *ACS Catal.*, 2015, **5**, 892-899.
- (25) L. T. Quertinmont and S. Lutz, *Tetrahedron*, 2016, **72**, 7282-7287.
- (26) E. D. Amato and J. D. Stewart, *Biotechnol. Adv.*, 2015, **33**, 624-631.
- (27) Y. A. Pompeu, B. Sullivan and J. D. Stewart, *ACS Catal.*, 2013, **3**, 2376-2390.
- (28) S. K. Padhi, D. J. Bougioukou and J. D. Stewart, *J. Am. Chem. Soc.*, 2009, **131**, 3271-3280.
- (29) M. W. Fraaije and A. Mattevi, *Trends Biochem. Sci.*, 2000, **25**, 126-132.
- (30) M. Kayikci, A. J. Venkatakrishnan, J. Scott-Brown, C. N. J. Ravarani, T. Flock and M. M. Babu, *Nat. Struct. Mol. Biol.*, 2018, **25**, 185-194.
- (31) D. Xu, R. M. Kohli and V. Massey, *Proc. Natl. Acad. Sci. U. S. A.*, 1999, **96**, 3556.
- (32) J. Guo, R. Zhang, J. Ouyang, F. Zhang, F. Qin, G. Liu, W. Zhang, H. Li, X. Ji, X. Jia, B. Qin and S. You, *ChemCatChem*, 2018, **10**, 5496-5504.
- (33) N. Nett, S. Duewel, A. A. Richter and S. Hoebenreich, *ChemBioChem*, 2017, **18**, 685-691.
- (34) D. J. Bougioukou, S. Kille, A. Taglieber and M. T. Reetz, *Adv. Synth. Catal.*, 2009, **351**, 3287-3305.
- (35) S. Daum, F. Erdmann, G. Fischer, B. Féaux de Lacroix, A. Hessamian-Alinejad, S. Houben, W. Frank and M. Braun, *Angew. Chem. Int. Ed.*, 2006, **45**, 7454-7458.
- (36) W. Tian, C. Chen, X. Lei, J. Zhao and J. Liang, *Nucleic Acids Res.*, 2018, **46**, W363-W367.
- (37) A. Z. Walton, W. C. Conerly, Y. Pompeu, B. Sullivan and J. D. Stewart, *ACS Catal.*, 2011, **1**, 989-993.

(38) A. Z. Walton, B. Sullivan, A. C. Patterson-Orazem and J. D. Stewart, *ACS Catal.*, 2014, **4**, 2307-2318.

(39) T. Hadi, A. Díaz-Rodríguez, D. Khan, J. P. Morrison, J. M. Kaplan, K. T. Gallagher, M. Schober, M. R. Webb, K. K. Brown, D. Fuerst, R. Snajdrova and G.-D. Roiban, *Org. Process Res. Dev.*, 2018, **22**, 871-879.